Hindawi
Geofluids
Volume 2018, Article ID 7049830, 17 pages
https://doi.org/10.1155/2018/7049830

Research Article

A Fluid-Solid Coupling Mathematical Model of Methane Driven by Water in Porous Coal

Bingxiang Huang and Weiyong Lu

State Key Laboratory of Coal Resources and Safe Mining, China University of Mining and Technology, Xuzhou, Jiangsu 221116, China

Correspondence should be addressed to Weiyong Lu; 489698551@qq.com

Received 30 April 2018; Revised 14 July 2018; Accepted 25 July 2018; Published 16 September 2018

Academic Editor: Joaquín Jiménez-Martínez

The existence of the water-driven-methane effect in gassy coal has been verified by field tests and laboratory experiments. However, a water-driven-methane mathematical model that considers methane adsorption and desorption has not yet been established. Based on the water-driven-methane process, a fluid-solid coupling mathematical model of methane driven by water is established. The model's reliability is verified by the results of a water-driven-methane physical experiment and by using a solution of the COMSOL Multiphysics software. The space-time distribution regularities of the pore pressure, water-methane two-phase saturation, and pore pressure gradient in the water-driven-methane process are analysed. The results reveal the following. (1) The water-driven-methane fluid-solid coupling mathematical model for porous coal is reliable. (2) In the water-driven-methane process, there is an increasing zone and a decreasing zone of pore pressure in the coal sample. The increasing zone of pore pressure is closest to the side of the water inlet, and its area gradually decreases. The decreasing zone of pore pressure is closest to the side of the methane outlet, and its area gradually increases. Over time, the methane pressure in the increasing zone of pore pressure first increases and then decreases, and the methane pressure in the decreasing zone of pore pressure continuously decreases. The change (increase or decrease) rate of the methane pressure gradually decreases from both ends towards the middle of the coal sample. (3) The curve of the water saturation over time changes from a lower concave curve to a straight line, while the curve of the methane saturation with time changes from an upper convex curve to a straight line. The methane saturation in the decreasing zone of pore pressure is greater than that in the increasing zone of pore pressure. Over time, the water saturation of a specific point in space continuously increases while its methane saturation continuously decreases. Both of the increase rate of the water saturation and the decrease rate of the methane saturation gradually reduce over time. (4) The pore pressure gradient along the driving direction first decreases and then increases. The decreasing zone of the pore pressure gradient is located in the increasing zone of pore pressure, and the increasing zone of the pore pressure gradient is located in the decreasing zone of pore pressure. Over time, the pore pressure gradient at the side of the water inlet increases, and its increase rate decreases. The pore pressure gradient at the side of the methane outlet decreases, and its decrease rate decreases. The rate of increase in the pore pressure gradient at the side of the water inlet is greater than the rate of decrease in the pore pressure gradient at the side of the methane outlet.

1. Introduction

During the process of water injection or hydraulic fracturing in gassy coal, the methane concentration of the airflow in the roadway clearly increases. This phenomenon is known as the water-driven-methane effect [1]. The existence of this phenomenon has been shown in laboratory experiments. The effect has both advantages and disadvantages in production practice. On the one hand, it can provide new ideas and technology for the exploitation of coalbed gas, and the hydraulic measures are used to eliminate methane outbursts. On the other hand, it can increase the methane concentration of the airflow in the roadway in addition to the methane content and methane pressure of the local region in the coal seam, which is detrimental to the prevention of coal and methane outbursts and methane explosions [2–7]. In fact, the negative

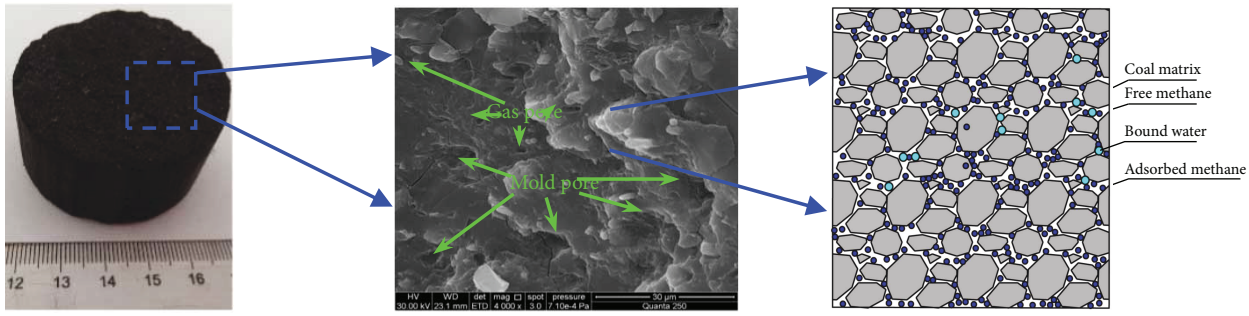

(a) Porous coal

(b) Pore structure under a scanning electron microscope

(c) Methane in the pore

Figure 1: Methane distribution in porous coal.

effect of the water-driven-methane process has always existed, but it has not been an obvious cause of a disaster and has not attracted the attention of fieldworkers and researchers. With an increase in the exploitation depth of coal seam gas and coal resources, the positive and negative impacts of the water-driven-methane effect have become more and more obvious [8, 9]. However, at present, a mathematical model considering the effect of methane adsorption and desorption in coal has not been established to describe the water-driven-methane effect in coal. Therefore, during the water-driven-methane process, the distribution regularities of water and methane saturation in addition to the pore pressure and its gradient are still not clear. Therefore, to describe the water-driven-methane process accurately, a mathematical model should be established. Based on this mathematical model, the distribution regularities of water and methane saturation and of the pore pressure and its gradient can be analysed. A more comprehensive and in-depth understanding of the effect of this process will be useful for making the best use of this phenomenon's advantages and overcoming its disadvantages.

At present, a mathematical model has been established to describe water-gas or water-oil two-phase driving processes in conventional porous medium reservoirs [10–12]. Of course, coal rock masses are also porous media. The water-driven-methane process in a coal rock mass also belongs to water-gas two-phase flow in porous media. However, the effect of methane adsorption and desorption in coal is significantly different from that of the water-driven-gas process in coal rock masses and conventional porous media. During the processes of water drainage, decreasing pressure, and desorption of coalbed methane, there is a stage of water-gas two-phase flow. A coupled fluid-solid mathematical model that considers the effects of methane adsorption and desorption has already been established to describe this stage, but it still cannot be directly used to describe the water-driven-methane process in coal because of the following reasons. (1) The coupled fluid-solid model of coalbed methane drainage is used to describe the process of water-methane two-phase flow with a decrease in the water pressure and adsorbed coalbed methane becoming free coalbed methane. However, a coupled fluid-solid model of methane driven by water is required to describe the process of driving out methane in coal by the injected water, which is injected into the coal. The boundary conditions of the above two processes are different. In addition, the injected water will also cause an increase in methane pressure, resulting in the transformation of free methane to adsorbed methane. (2) For the coupled fluid-solid mathematical models of coalbed methane drainage, some equations are only listed but not solved, and for the other equations, only the numerical solutions are offered. However, the reliability of these mathematical models has not been verified. Furthermore, these models primarily study the evolution regularities of reservoir permeability and methane production but rarely address the distribution regularities of water-methane two-phase saturation and of the pore pressure and its gradient [13–15].

To clarify the distribution regularities of water-methane two-phase saturation and the pore pressure and the mechanism of the pore pressure gradient in the water-driven-methane process, pure porous coal rock without fractures is selected in this study, thereby excluding the effects of fractured structures. Based on the elastic theory of porous media, the principle of effective stress, the principle of methane adsorption and desorption, and the principle of conservation of mass and Darcy's law, a coupled fluid-solid mathematical model of methane driven by water is established. This model considers the effect of coalbed methane adsorption and desorption, the deformation field of the coal rock mass, and the seepage field of water and methane. The reliability of the mathematical model is verified by physical experiments of artificially suppressed briquette coal. On the basis of the mathematical model, a further study is developed on the distribution regularities of water-methane two-phase saturation and the pore pressure and the mechanism of the pore pressure gradient. Scientific understanding is provided for the water-driven-methane process in the porous coal.

2. Conceptual Model

Porous coal rock (Figure 1(a)) is characterized by a pore structure of air pores and mold pores and similar structures (Figure 1(b)), which can provide space for free methane and adsorbed methane (Figure 1(c)) [16–18]. In a porous coal rock, there are many interconnected pores, which can be regarded as the migration channels of fluid [19, 20].

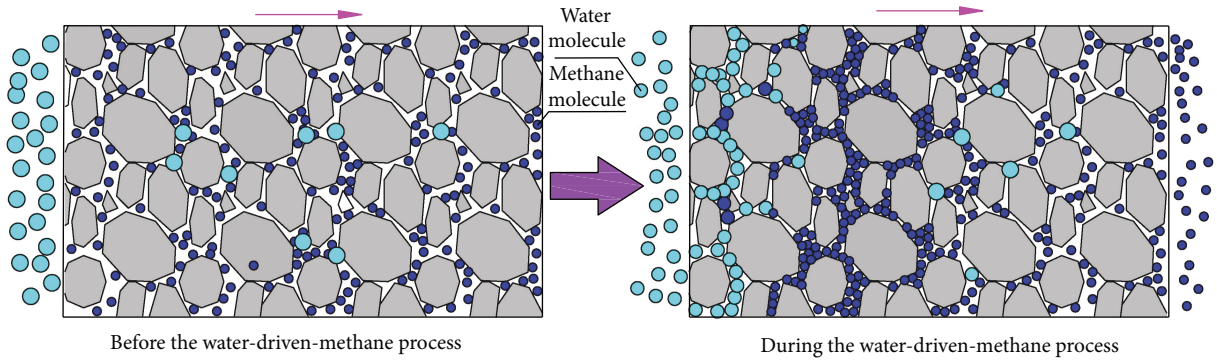

Figure 2: Conceptual model of methane driven by water in porous coal rock.

Before methane is driven by water, there are primarily methane and a small amount of bound water (Figure 1(c)) in the pores of coal rock. The pressure is regarded as the initial pore pressure. During the water-driven-methane process, pressure water will flow along the pore channel [21–24]. This breaks the original mechanical equilibrium in the coal sample, and the stress is redistributed again. The methane pressure will rise at a distance from the water injection position. The water drives the methane in the pore to move forward in the pore channel until the methane is expelled from the coal rock mass. At the same time, the pore space of methane is also occupied by water [1]. The pore space occupied by water forms the water zone, but a certain amount of methane remains in the water zone. The pore space occupied by methane forms the gas zone, and there is also a small amount of bound water in the gas zone. According to the above process, a conceptual model of methane driven by water in porous coal rock (Figure 2) is constructed in this study.

3. Mathematical Model

3.1. Basic Assumptions. The mathematical model is established based on the following six basic assumptions:

(1) The water-methane two-phase flow is an immiscible system, and the solubility of methane in water is not considered in the model.

(2) The temperature in the seepage field is a constant, and the water, methane, and rock strata are in a state of thermal equilibrium.

(3) Methane is an ideal gas. The flow of water and methane in porous coal is both characterized by laminar flow and obeys Darcy's law.

(4) Porous coal rock is homogeneous and isotropic. Its solid skeletons and pores are compressible, and the deformation of porous coal rock is elastic and small.

(5) The influences of capillary pressure and gravity are considered in the mathematical model.

(6) Only the water-driven-methane effect is considered, and the water-displaced-methane effect is ignored.

3.2. Basic Equations

3.2.1. The Equations of the Stress Field. The free coalbed methane and water in the coal can transfer fluid pressure. When methane is adsorbed on the surface of the coal, the surface tension of the coal decreases, resulting in the expansion of the volume. However, when the methane is desorbed from the coal surface, its volume shrinks. The above differences have prompted scholars to supplement the Terzaghi's effective pressure principle to adapt to the deformation of coal, which is rich in adsorbed coalbed methane. Based on the elastic theory of porous media, the constitutive equation of the coal body considering the effect of methane adsorption and desorption is as follows [14]:

$$\varepsilon_{ij} = \underbrace{\frac{1}{2G}\sigma_{ij} - \left(\frac{1}{6G} - \frac{1}{9K}\right)\sigma_{kk}\delta_{ij}}_{\text{Geostress strain}} + \underbrace{\frac{\alpha_p}{3K}p\delta_{ij}}_{\text{Pore pressure strain}} + \underbrace{\frac{\varepsilon_a}{3}\delta_{ij}}_{\text{Adsorption swelling strain}}, \tag{1}$$

in which

$$\begin{aligned} G &= \frac{E}{2(1+\nu)}, \\ \sigma_{kk} &= \sigma_{11} + \sigma_{22} + \sigma_{33}, \\ \alpha_p &= \frac{1-K}{K_s}, \\ K &= \frac{2G(1+\nu)}{3(1-2\nu)} = \frac{E}{3(1-2\nu)}, \\ K_s &= \frac{E_s}{1-2\nu}, \\ \varepsilon_a &= \varepsilon_g V_g = \varepsilon_g \frac{V_L p_g}{p_g + P_L}, \\ p &= S_w p_w + S_g p_g, \end{aligned} \tag{2}$$

where G is the shear modulus, E is the elastic modulus, ν is Poisson's ratio, σ_{kk} represents the components of the normal stress, p is the pore pressure, $\alpha(\leq 1)$ is Biot's effective stress

coefficient, K is the volume modulus of coal rock, K_s is the volume modulus of a coal rock skeleton, E_s is the elastic modulus of a coal rock skeleton, δ_{ij} is the Kronecker symbol (when i is equal to j, δ_{ij} is 1; when i is unequal to j, δ_{ij} is 0), ε_s is the adsorption strain of the methane, ε_g is the adsorption strain coefficient of the methane, P_L is the Langmuir pressure constant, V_L is the Langmuir volume constant, S_w is the water saturation, p_w is the pore pressure of water, S_g is the methane saturation, and p_g is the pore pressure of methane.

According to the theory of elastic mechanics, the relation between strain and displacement is

$$\varepsilon_{ij} = \frac{1}{2}\left(u_{i,j} + u_{j,i}\right). \tag{3}$$

From the condition of static equilibrium, the following can be obtained:

$$\sigma_{ij,j} + F_i = 0. \tag{4}$$

Substituting (1), (2), and (3) into (4), the modified Navier balance equation (5) with the displacement as the fundamentally unknown quantity and with the coupling term included can be obtained.

$$Gu_{i,jj} + (G+\lambda)u_{j,ji} - \alpha_p p_i - K\varepsilon_{a,i} + F_i = 0, \tag{5}$$

where u_i is the displacement along the i direction and F_i is the volume force along the i direction $(i = x, y, z)$.

3.2.2. Mass Conservation Equation. There are adsorbed methane and free methane in coal. The methane, which is initially adsorbed on the internal surface of matrix pores, becomes free-phase methane due to the reduction in pore pressure. On the contrary, with the increase in the pore pressure, the free-phase methane can become adsorbed methane.

The total methane can be calculated by

$$m_g = m_y + m_x, \tag{6}$$

where m_y is the free methane and m_y is the adsorbed methane.

The free methane content m_y can be calculated by the following:

$$m_y = \rho_g \varphi_{nw}, \tag{7}$$

where ρ_g is the density of methane and φ_{nw} is the porosity of coal rock.

By regarding the methane as an original gas, the relationship between its density and pressure can be expressed as follows:

$$\rho_g = \beta p_g, \tag{8}$$

where p_g is the methane pressure (Pa), $\beta = M_g/RT$ is the compression coefficient (kg/(m^3·Pa)), M_g is the molecular weight of methane (kg/mol), R is the ideal gas constant (3.814 kJ/(mol·K)), and T is the absolute temperature (K).

According to (8) and (9), the density of methane can be calculated by

$$\rho_g = \frac{p_g}{p_0}\rho_0, \tag{9}$$

where p_0 is the pressure under standard conditions (101325 Pa) and ρ_0 is the density of methane under standard conditions (0.717 kg/m^3).

The adsorbed methane content m_x satisfies the Langmuir formula, whose corresponding equation is

$$m_x = \frac{ab\beta p_0 \rho_c}{1 + bp_g} p_g, \tag{10}$$

where a is the ultimate adsorption capacity of the methane (m^3/kg), b is the adsorption equilibrium constant of the methane (Pa^{-1}), and ρ_c is the density of coal (kg/m^3).

According to the principle of mass conservation, the mass continuity equation of a fluid is expressed as follows:

$$\frac{\partial m_i}{\partial t} + \nabla \cdot (\rho_i \cdot u_i) = 0, \tag{11}$$

$$u_i = -\lambda_i(\nabla \rho_i + \rho_i g \nabla D), \tag{12}$$

where i represents w or g, where w is a water phase and g is a methane phase; m_i is the mass of an i-phase fluid (kg/m^3); ρ_i is the mass of an i-phase fluid (kg/m^3); u_i is the average velocity of an i-phase fluid (m/s); K is the absolute permeability of the coal (m^2); $\lambda_i = K k_{r,i}/\mu_i$ is the conductivity of an i-phase fluid; $k_{r,i}$ is the relative permeability of an i-phase fluid; μ_i is the dynamic viscosity of an i-phase fluid (Pa·s); and D is the height of the coordinate system (m).

By regarding the methane as a compressible fluid and the water as an incompressible fluid, with the union of (1), (2), (3), (4), (5), (6), (7), (8), (9), (10), (11), and (12), the mass continuity equation of the methane and water can be separately expressed as follows:

$$\begin{aligned} &\beta p_g S_g \frac{\partial \varphi}{\partial t} + \varphi \beta p_g \frac{\partial S_g}{\partial t} + \left(\varphi \beta S_g + \frac{ab\beta p_0 \rho_c}{\left(1 + bp_g\right)^2}\right)\frac{\partial p_g}{\partial t} \\ &\quad - \nabla \cdot \left[\beta p_g \lambda_g \left(\nabla p_g + \rho_g g \nabla D\right)\right] \\ &= 0, \frac{\partial(\varphi S_w)}{\partial t} - \nabla \cdot [\lambda_w(\nabla p_w + \rho_w g \nabla D)] \\ &= \varphi \frac{\partial S_w}{\partial t} + S_w \frac{\partial \varphi}{\partial t} - \nabla \cdot [\lambda_w(\nabla p_w + \rho_w g \nabla D)] = 0. \end{aligned} \tag{13}$$

For a further simplification, (13) can be separately expressed as follows:

$$\varphi\frac{\partial S_w}{\partial t}-\nabla\cdot[\lambda_w(\nabla p_w+\rho_w g\nabla D)]=-S_w\frac{\partial\varphi}{\partial t},$$
$$\varphi\beta p_g\frac{\partial S_g}{\partial t}+\left(\varphi\beta S_g+\frac{ab\beta p_0\rho_c}{\left(1+bp_g\right)^2}\right)\frac{\partial p_g}{\partial t}$$
$$-\nabla\cdot\left[\beta p_g\lambda_g\left(\nabla p_g+\rho_g g\nabla D\right)\right]=-\beta p_g S_g\frac{\partial\varphi}{\partial t}. \tag{14}$$

3.2.3. Level Set Transport Equation. The level set method, firstly proposed by Osher and Sethian, is a numerical method for solving the two-phase flowing equations including the surface tension phase. It can be utilized to simulate the water-driven-gas process. To understand the dynamic change characteristics of water and gas two-phase flow, the method has the advantages of convenience, visualization, and the like. The level set equation is written as follows [25]:

$$\frac{\partial\phi}{\partial t}+u\cdot\nabla\phi=\gamma\nabla\cdot\left(\varepsilon\nabla\phi-\phi(1-\phi)\frac{\nabla\phi}{|\nabla\phi|}\right), \tag{15}$$

where ϕ is a contour line of the water-gas two-phase interface, γ is the reinitialization parameter in the solution of the equation, u is the velocity of the fluid, ε is the thickness of the water-gas interface, and t is the time of water and gas flow.

To avoid the instability of the numerical calculation, the density and viscous property parameters of the fluid in the vicinity of the interface need to be smoothed. The smoothing method of the level set equation describes the changes in the density and dynamic viscosity in the process of water-gas two-phase flow with the level set function, and the corresponding equations are

$$\rho(\phi)=\rho_g+\left(\rho_w-\rho_g\right)\phi,$$
$$\mu(\phi)=\mu_g+\left(\mu_w-\mu_g\right)\phi, \tag{16}$$

where ρ_w and ρ_g are the densities of water and gas (kg/m^3), respectively, and μ_w and μ_g are the dynamic viscosities of water and methane (Pa·s), respectively.

3.2.4. Dynamic Model of Porosity and Permeability. Methane migration is determined by the porosity and permeability of coal rock, which are a bridge between the stress field and seepage field. Both of these key parameters are closely related to the stress and inherent material properties of coal rock.

Porous coal rock is porous media. Its porosity is influenced by the pore pressure and matrix expansion/contraction caused by methane adsorption/desorption. Considering the combined effect of the pore pressure and matrix expansion/contraction, the dynamic model of porosity can be written as follows [26, 27]:

$$\varphi=\frac{1}{1+S}[\varphi_0(1+S_0)+\alpha(S-S_0)], \tag{17}$$

in which

$$S=\frac{\varepsilon_v+p}{K_s-\varepsilon_a},$$
$$S=\frac{\varepsilon_{v0}+p_0}{K_s-\varepsilon_{a0}}, \tag{18}$$
$$\varepsilon_v=\varepsilon_x+\varepsilon_y+\varepsilon_z,$$

where φ is the initial porosity of coal rock; ε_v is the volume strain of coal rock; ε_x, ε_y, and ε_z are the volume strain in the x, y, and z directions, respectively; K_s is the volume modulus of the coal skeleton; and the index 0 is the initial value of the corresponding parameter.

The absolute permeability of porous media is also influenced by the in situ stress. The dynamic model of absolute permeability can be expressed as follows [28, 29]:

$$K=\frac{K_0}{1+\varepsilon_v}\left[1+\frac{\varepsilon_v-\Delta p(1-\varphi_0)/K_s}{\varphi_0}\right]^3, \tag{19}$$

where K_0 is the initial permeability of the porous media.

Capillary pressure curves are used by the Brooks and Corey-Burdine model to calculate the relative permeability of a fluid in porous media. Based on the Brooks and Corey-Burdine model, the relative permeabilities of water and methane in porous coal rock are a function of the water saturation. The corresponding expressions are as follows [30]:

$$k_{r,w}=k_{r,w0}\left(\frac{S_w-S_{r,w}}{1-S_{r,w}-S_{r,g}}\right)^{3+2/\lambda},$$
$$k_{r,g}=k_{r,g0}\left(1-\frac{S_w-S_{r,w}}{1-S_{r,w}-S_{r,g}}\right)^2\left[1-\left(\frac{S_w-S_{r,w}}{1-S_{r,w}-S_{r,g}}\right)^{1+2/\lambda}\right], \tag{20}$$

where $k_{r,w0}$ is the relative permeability of the water phase endpoints, $k_{r,g0}$ is the relative permeability of the gas phase endpoint, $S_{r,w}$ is the residual saturation of the water phase, $S_{r,g}$ is the residual saturation of the gas phase, and λ is a parameter that represents the pore structure characteristics of porous media.

When the parameter λ of the Brooks and Corey-Burdine model is 1, the calculated relative permeability curves of water and methane are consistent with the results of the unsteady method experiment, as shown in Figure 3 [31].

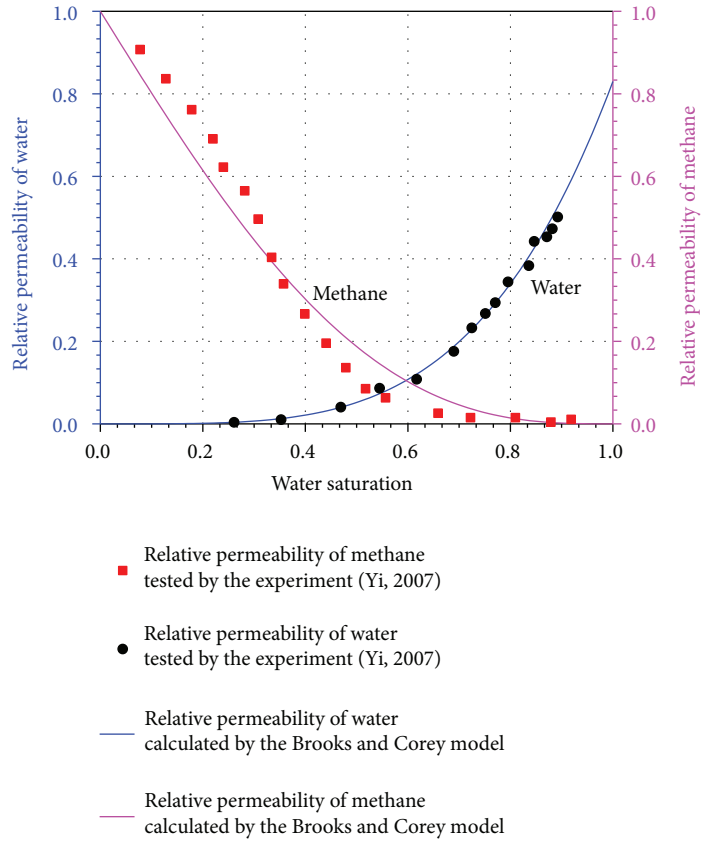

Figure 3: The permeability of water and methane in porous coal rock.

3.2.5. Capillary Equation. When the two immiscible fluids of water and gas flow into the pore channel, a meniscus-shaped interface between the water and methane is formed. The pressure on both sides of the interface is discontinuous. The difference in the pressure is called the capillary force, and the corresponding expression is

$$p_{cgw} = p_g - p_w, \tag{21}$$

where p_{cgw} is the capillary force, p_g is the methane pressure, and p_w is the water pressure.

3.2.6. Saturation Equation. In saturated porous media, the effective pores are all filled with water and gas. This process is described by the saturation equation:

$$S_g + S_w = 1. \tag{22}$$

3.3. Geometric Model and Boundary Conditions. After water enters the coal rock from the borehole, it will drive the methane forward along the pore channels in the coal rock. The boundary and initial conditions corresponding to the physical model are as follows:

$$\begin{aligned} p_w &= p_w(t), \quad \partial\Omega \text{ inlet surface}, \\ p_g &= p_{g0}, \quad \partial\Omega \text{ outlet surface}, \\ n \cdot \rho_w[-\lambda_w(\nabla p_w + \rho_w g \nabla D)] &= 0, \quad \partial\Omega \text{ side of the cylinder}, \\ n \cdot \rho_g\left[-\lambda_g\left(\nabla p_g + \rho_g g \nabla D\right)\right] &= 0, \quad \partial\Omega \text{ side of the cylinder}, \\ p &= p_0, \quad \partial\Omega. \end{aligned} \tag{23}$$

4. Experimental Verification of the Model

4.1. Experiment of Methane Driven by Water in Porous Coal Rock

4.1.1. Experimental System. Based on the principle of methane displaced by water, a pseudo three-axial experimental system of water-methane displacement (Figure 4) is developed. This experimental system can simulate the process of displacing methane by water under the conditions of axial and confining pressures on a cylindrical coal sample with a diameter of 50 mm and a height of 100 mm. The experimental system comprises an axial and confining pressure loading system, a water injection system, a gas injection system, and displaced gas collection and measurement devices. The principle and real objective of the water-methane displacement device are shown in the blue rectangular dashed frame in Figure 4. The axial pressure is loaded by the hydraulic jack at the bottom of the water-methane displacement device, and the confining pressure is applied by injecting hydraulic oil into the annular space. The water pressure loading is controlled by a four-channel, electrohydraulic servo control

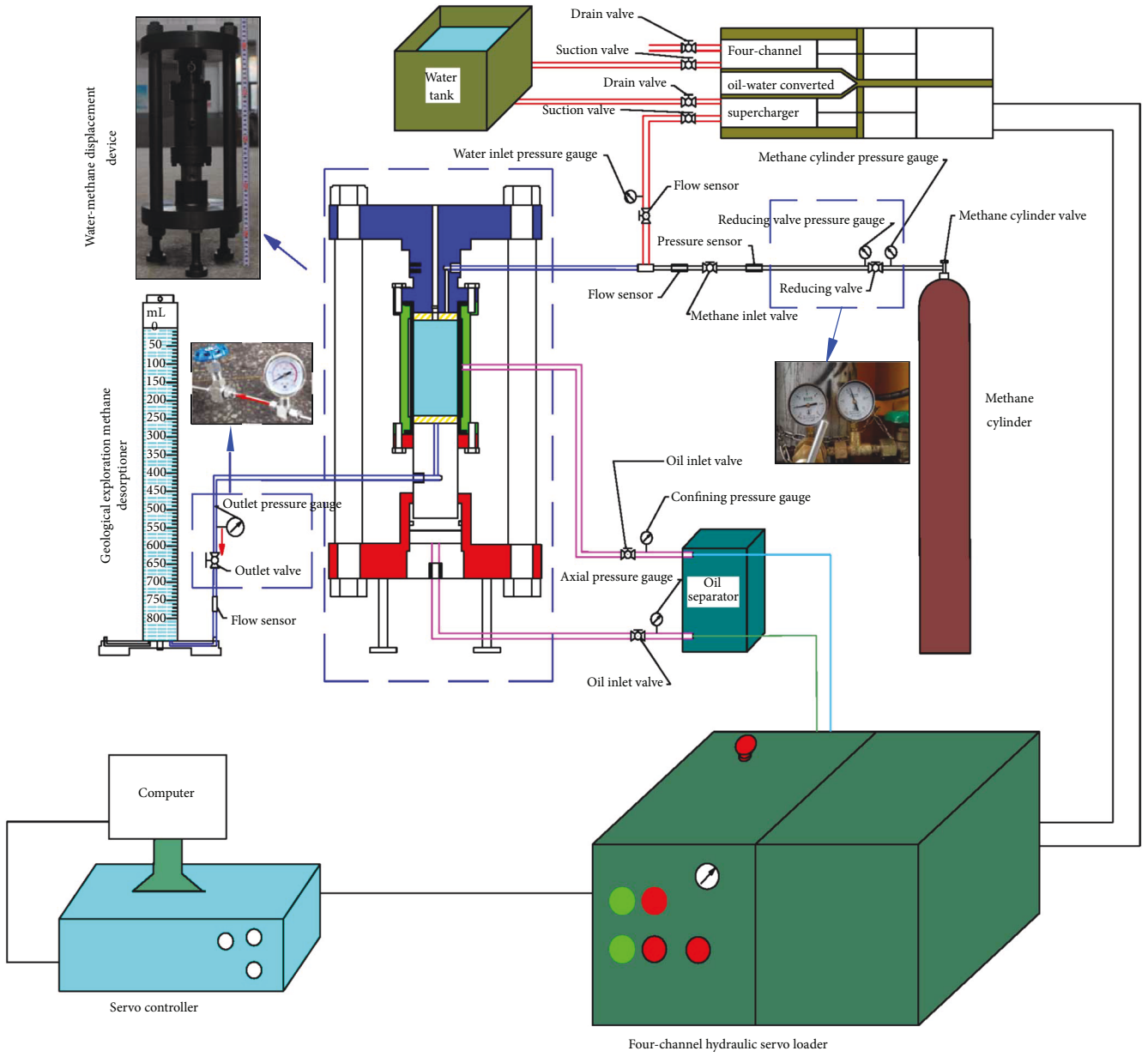

Figure 4: Experimental system of methane displacement by water.

system based on the MOOG valve. The pressure of the gas circuit system is adjusted using the pressure release valve at the outlet of the methane cylinders. The collection and volumetric measurement of the displaced methane are completed with the help of a geological exploration methane desorption instrument.

4.1.2. Preparation of the Briquette Coal. Briquette coal is formed from coal powder under the pressure provided by a rigid pressure testing machine, and the internal structure of the briquette coal is porous. To avoid the influence of discrete factors such as joints and fissures, the briquette coal can be an ideal porous coal. The preparation processes used for the briquette coal in this paper (Figure 5) are as follows. First, sieve out the coal powder with diameters of 0.3~0.45 mm with a sifter (Figure 5(a)). Mix the coal powder and water to achieve a mass ratio of 10 : 1, and then put the coal-water mixture into the mold (Figure 5(b)). Exert a pressure of 100 MPa (Figure 5(b)) on the coal-water mixture with a rigid pressure testing machine. After ejection (Figure 5(c)), a briquette coal sample with a diameter of 50 mm and a height of 100 mm is produced (Figure 5(d)).

4.1.3. Experimental Process. The processes of the water-displaced-methane experiment are as follows. (1) Load the axial and confining pressures. An axial pressure of 2 MPa and a confining pressure of 1 MPa are simultaneously applied at loading rates of 0.2 MPa/s and 0.1 MPa/s, respectively. Then, maintain the axial pressure of 2 MPa and the confining pressure of 1 MPa for 5 minutes. (2) Vent the air. Open the

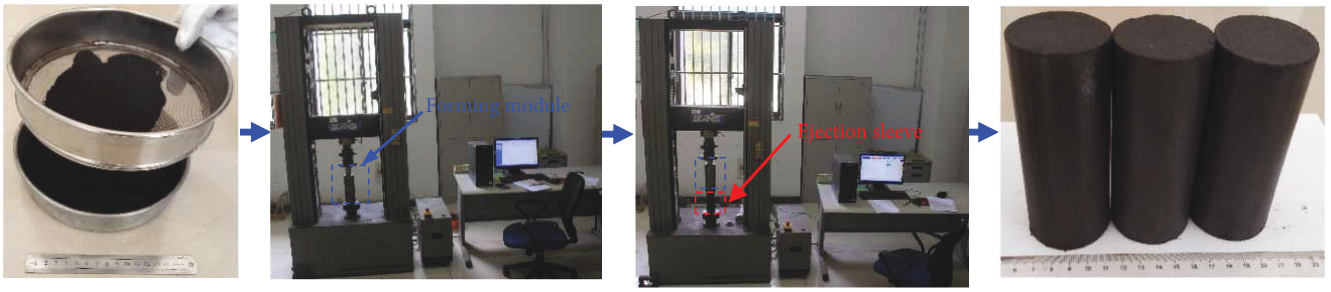

(a) Sieve coal powder (b) Compression with a pressure testing machine (c) Module release (d) Briquette coals

Figure 5: Preparation process of the briquette coal samples.

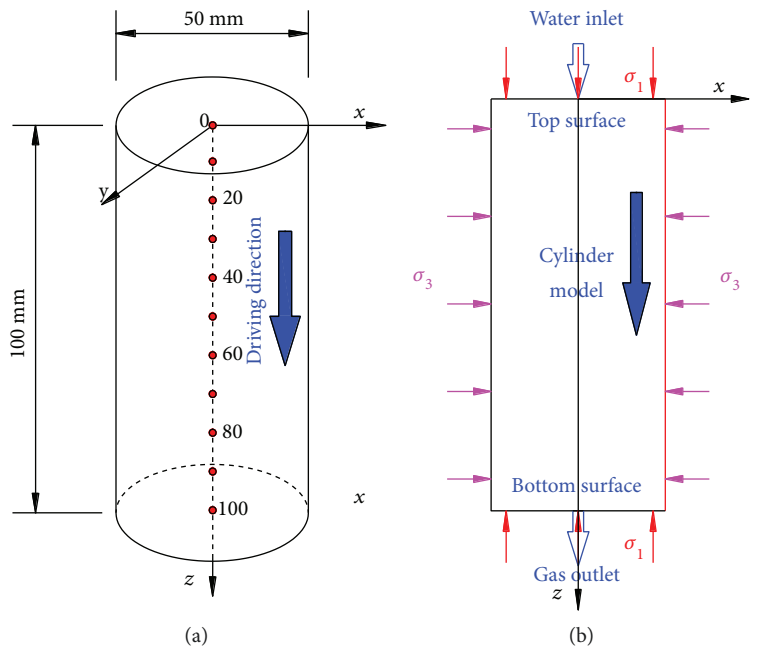

(a) (b)

Figure 6: Schematic diagram of the geometric model (a) and imposed constraints (b).

intake and outlet valves and collect the gas at the outlet. When the methane concentration of the collected gas is close to 100%, it is believed that the air in the experimental system has been vented out. Then, close the outlet valve. (3) Achieve methane adsorption and desorption equilibrium. Open the cylinder and inlet valves and control the output pressure of the cylinder by adjusting the pressure-reducing valve. The coal sample finally arrives at a state of adsorption and desorption equilibrium, and the corresponding methane pressure is 0.5 MPa. (4) Drive the methane by water injection. Close the gas inlet valve, and open the gas outlet and water inlet valves. Maintain a water pressure of 0.7 MPa, and inject water into the coal sample. Collect the methane displaced by water until no further methane is released.

4.2. Calculation of the Mathematical Model

4.2.1. Geometrical Model. A cylindrical model with a diameter of 50 mm and a height of 100 mm (Figure 6(a)) is adopted in this numerical simulation. To facilitate the monitoring and analysis of the related parameters of the postprocessing model, the water-displaced-methane direction is flagged as the positive direction of the z-axis, along which nine monitoring points are separately distributed at the locations of 10 mm, 20 mm, 30 mm, 40 mm, 50 mm, 60 mm, 70 mm, 80 mm, and 90 mm from the top of the cylinder. At the same time, the axis of the cylinder is selected as the monitoring line. Water enters the coal sample from its top and drives the methane in the coal forward. The side of the cylinder is an impermeable boundary, the upper surface is the water inlet, and the lower surface is the methane outlet. In the water-displaced-methane process, the loading conditions of the axial and confining pressures are shown in Figure 6(b).

4.2.2. Determining the Parameters of the Numerical Simulation. The process of solving the equations using the COMSOL Multiphysics software is actually a recurrence of a physical process. The recurrence of a physical process needs to be built on the basis of a series of reasonable parameters.

Table 1: Parameters of the numerical simulation.

Symbol	Physical significance	Value	Unit
E	Elastic modulus of the coal rock	2713	MPa
E_s	Elastic modulus of the coal skeleton	8469	MPa
v	Poisson's ratio of the coal rock	0.32	1
φ_0	Initial porosity	0.09	1
μ_{nw}	Dynamic viscosity of the methane	$1.84e-5$	Pa·s
μ_w	Dynamic viscosity of the water	$1.01e-3$	Pa·s
ρ_s	Density of the coal skeleton	1470	kg/m^3
ρ_w	Density of water	1000	kg/m^3
K_0	Absolute permeability of the coal rock	$2e-17$	m^2
a	Langmuir ultimate adsorption capacity of the methane	0.036	m^3/kg
b	Langmuir adsorption equilibrium constant of the methane	3.304	MPa
$S_{r,w}$	Bound water saturation	0.2	1
$S_{r,g}$	Residual methane saturation	0.1	1
$k_{r,w0}$	Relative permeability of the water endpoint	0.83	1
$k_{r,g0}$	Relative permeability of the methane endpoint	1	1
p_{g0}	Outlet pressure	0.1	MPa
p_0	Initial pore pressure	0.5	MPa

Only in this way can the solution of the equations converge and the recurrence of the physical process succeed. To ensure that the numerical simulation is similar to the real physical experiment, the real physical parameters of the experimental briquette coal sample are used in the numerical calculation to the farthest extent possible. The relevant parameters used in this numerical simulation are shown in Table 1.

4.3. Comparisons of the Experiment and Numerical Calculation Results. The methane driven by water is mainly free methane in the coal. The free methane includes the original free methane (black line in Figure 7) and the desorbed methane from the adsorbed methane (magenta line in Figure 7). When pressure water enters the pores of the coal, the free methane in the pores will be driven forward along the seepage direction of the pressure water. As more water enters the pores, additional methane is driven by the water. It can be seen from Figure 7 that, during the initial 20 min, the collected methane volume of the water-displaced-methane experiment is significantly higher than the value calculated by the mathematical model; however, from 20 min to 60 min, the collected methane volumes of the experiment and numerical calculation gradually converge. In an hour, the collected methane volume of the water-displaced-methane experiment is 1.4 percent higher than that of the numerical calculation. This is because after water enters the coal, both the free methane in the pores and the free methane from the adsorbed methane displaced by water are driven out at the same time. Although only a small volume of the methane is displaced by water, its existence is confirmed by the experiment [1, 32–35]. Currently, the methane displaced by water cannot be quantitatively calculated by the mathematical formula. In this paper, the mathematical model also lacks a quantitative expression of the methane volume. This is the reason for the subtle difference between the experimental and calculation results. Overall, the results indicate that the mathematical model of the methane driven by water is basically reliable and can be used to predict the methane volume in the water-driven-methane process.

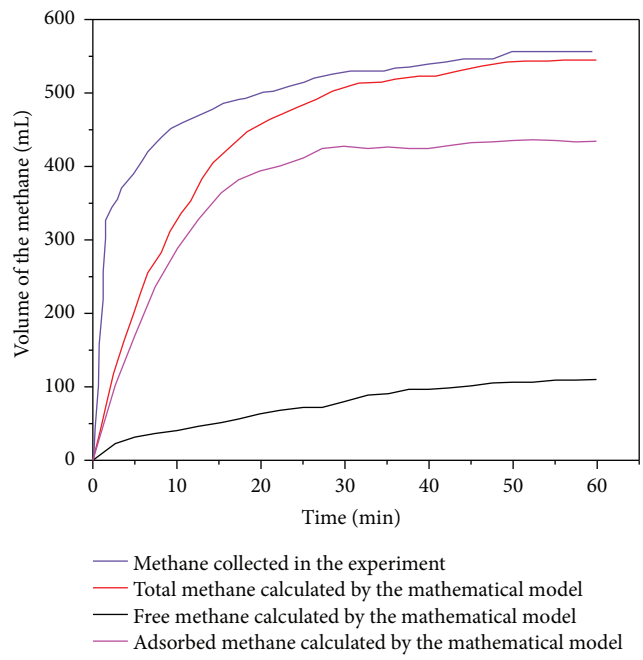

Figure 7: Change in the methane volume over time.

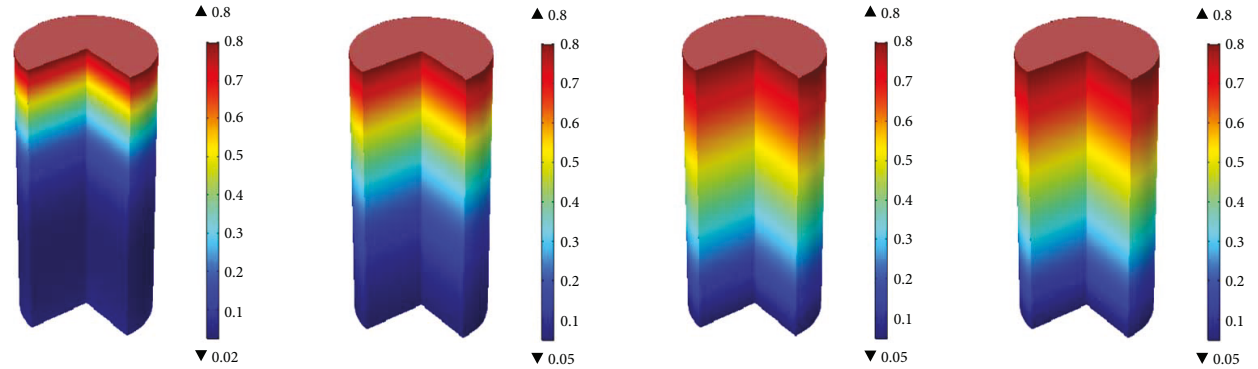

(a) Distribution cloud image of the water saturation

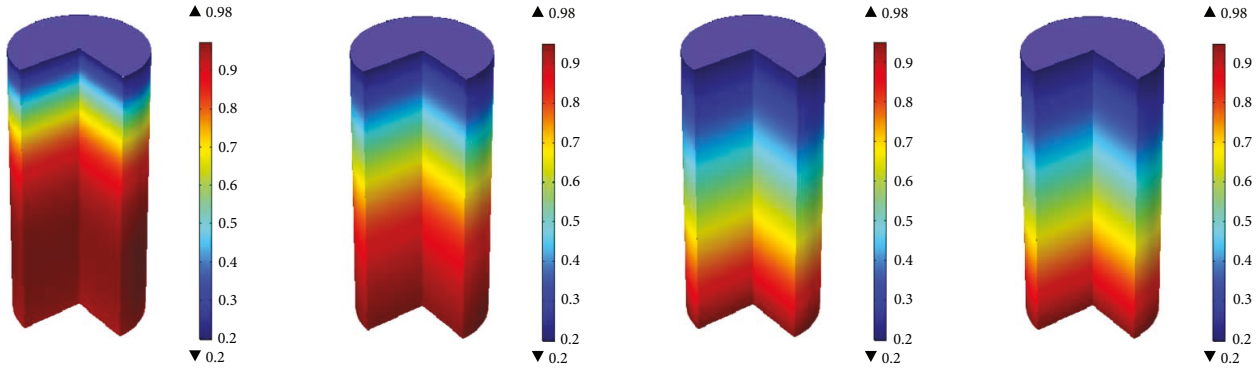

t=1 min t=5 min t=10 min t=30 min

(b) Distribution cloud image of the methane saturation

Figure 8: Space-time distribution of the water-methane two-phase saturation.

5. The Regularities of Methane Driven by Water

5.1. Space-Time Distribution Regularities of the Water-Methane Two-Phase Saturation

5.1.1. Visualization of the Space-Time Distribution of the Water-Methane Two-Phase Saturation along the Driving Direction. In the water-driven-methane process, the dynamic processes of the spatial distributions of water and methane saturations can be shown clearly by a saturation cloud image. The spatial distributions of the water and methane saturations at the four moments of 1 min, 5 min, 10 min, and 30 min are shown in Figure 8. The following can be seen from Figure 8. (1) When water enters the pores, the methane cannot be expelled completely, and there is residual methane in the pores of the coal rock. The residual methane saturation is set as 0.2 in the numerical simulation, so the maximum water saturation is 0.8. When the water saturation of the coal sample reaches 0.8, it is believed that the pores in this area have been saturated with water. (2) There is bound water in the coal sample. With the existence of bound water, the pores in the coal rock cannot be completely filled with methane. Therefore, the saturation of bound water in the coal sample is set as 0.05, and the maximum methane saturation is 0.95.

The results shown in Figure 8 are in agreement with the preset parameters of the mathematical model, which indicates indirectly the feasibility and reliability of the mathematical model. With the help of the COMSOL Multiphysics software, the visualization of the water-driven-methane behaviours can be realized. This contributes to the semiqualitative and semiquantitative research on the visualization of the space-time distribution of water-methane two-phase saturation.

5.1.2. Space-Time Distribution of the Water-Methane Two-Phase Saturation on the Axial Monitoring Line along the Driving Direction. When the pressure water is injected into the coal sample, more and more space is occupied by water. Meanwhile, the methane at that point is driven forward by water, resulting in a decrease in the space occupied by methane. Because the sum of the water and methane saturation at any space point is 1, the change regularities of the water and methane saturations at any point in space are opposite to one another. In other words, the water saturation is greater and the methane saturation is smaller, which is closer to the water inlet end. It can be seen from Figure 9. (1) In the same position, the water saturation increases with an increase in time (e.g., the water saturation at the 20 mm position increases from 0.05 to 0.65 within 30 minutes), but the methane saturation decreases over time (e.g., the methane saturation at the 20 mm position decreases from 0.95 to 0.35 within 30 minutes). Meanwhile, the increase rate of the water saturation decreases gradually, and the decrease rate of the methane saturation decreases gradually as well. The increase rate of the spatial distribution of the water saturation in 1~5 min is

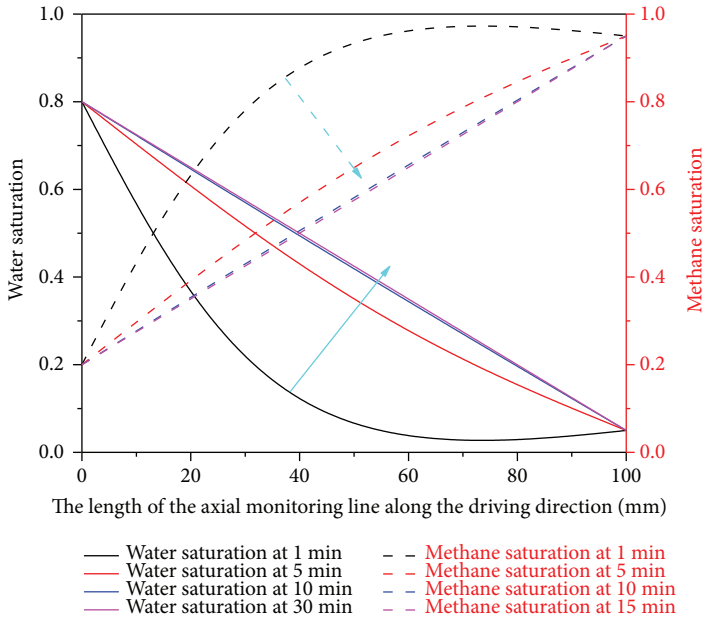

Figure 9: Space-time distribution curve of the water-methane two-phase saturation along the driving direction.

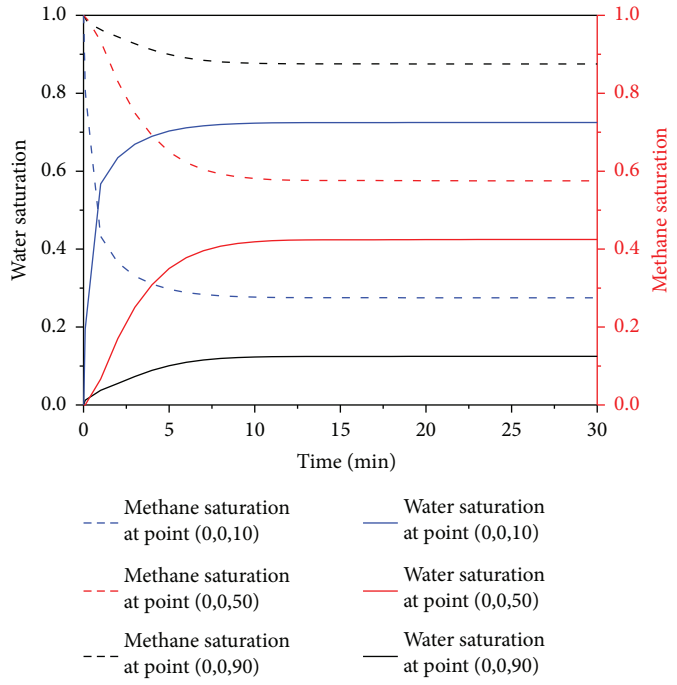

Figure 10: Space-time distribution curve of the water-methane two-phase saturation at the axial monitoring points along the driving direction.

larger than that in 10~30 min. (2) At the same time, the water saturation along the driving direction is continuously decreasing within the change interval from 0.05 to 0.8, and the methane saturation shows a continuous increase within the change interval from 0.2 to 0.95. (3) Over time, the curve of the water saturation changes from a lower concave curve to a straight line, and the curve of the methane saturation changes from an upper convex curve to a straight line. It is shown that with the continuous water-driven-methane process, the water saturation along the driving direction shows a linear increase and the methane saturation shows a linear decrease.

5.1.3. Space-Time Distribution of the Water-Methane Two-Phase Saturation at the Axial Monitoring Points along the Driving Direction. It can be seen from Figure 10 and Table 2 that the space-time distribution regularities of the water saturation are as follows. (1) For the same point in

Table 2: Space-time distribution of the water-methane two-phase saturation at the axial monitoring points.

Time (min)	Monitoring point (mm) 10 Saturation		50 Saturation		90 Saturation	
	Water	Methane	Water	Methane	Water	Methane
0	0.05	0.95	0.05	0.95	0.05	0.95
5	0.703	0.297	0.350	0.650	0.101	0.899
10	0.723	0.277	0.419	0.581	0.123	0.877
15	0.725	0.275	0.424	0.576	0.125	0.875

space, the water saturation first presents a nearly linear increase to a certain value and then remains stable. This is because, over time, water continues to flow into the coal sample, resulting in a continuous increase in the water saturation. However, the pore space at this point is limited. When the pore space is completely occupied by water, the water saturation at that point gradually becomes saturated and reaches a stable value. (2) The increased values of the water saturation at 10 m at 0~5 min, 5~10 min, and 10~15 min are, respectively, 0.653, 0.02, and 0.002, which indicates that the increase in the rate of water saturation gradually reduces over time. The changes in the water saturation at the 50 m and 90 m positions follow the same regularities as that at the 10 m position.

It can be seen from Figure 10 that the space-time regularities of the methane saturation are as follows. (1) For the same point in space, the methane saturation first presents a nearly linear decrease to a certain value and then remains stable. This is because, over time, pressure water enters the coal sample, drives the methane out from the coal sample, and occupies the pore space of the methane. However, the total pore space of the coal has a certain value. With an increase in the water entering the coal sample, the pore space occupied by water gradually increases and the pore space occupied by methane gradually decreases. When the pore space occupied by water in the coal sample tends to be stable, the pore space occupied by the methane will eventually stabilize. (2) The decreasing values of the methane saturation at the 10 m position at 0~5 min, 5~10 min, and 10~15 min are 0.653, 0.02, and 0.002, respectively. This indicates that, over time, the decreasing rate of methane saturation gradually reduces. The changes in the methane saturation at the 50 m and 90 m positions follow the same regularities as that at the 10 m position. (3) At the same time, the methane saturation is lower, which is closer to the water inlet. This is because the water injection volume at a specific time is certain. The closer to the water inlet, the greater the pore space occupied by water and the lower the pore space occupied by methane.

5.2. Space-Time Distribution Regularities of the Pore Pressure

5.2.1. Space-Time Distribution of the Pore Pressure along the Driving Direction. The following can be seen from Figure 11. (1) The initial pore pressure in the coal sample is 0.5 MPa. However, in the water-driven-methane process, the pore pressure in the coal sample is no longer 0.5 MPa. This indicates that, in the water-driven-methane process, the pore pressure in the coal sample is redistributed. Compared with the initial pore pressure of 0.5 MPa, the maximum pore pressure after redistribution is 0.7 MPa and the minimum pore pressure after redistribution is 0.1 MPa. This shows that there is only a range of increasing zones of pore pressure caused by the transmission of water pressure. (2) Using the initial pore pressure of 0.5 MPa as the dividing line, the coal sample can be divided into an increasing zone and a decreasing zone of pore pressure, as shown by the dotted lines with arrows in Figure 11. Over time, the increasing zone of pore pressure gradually decreases, but the decreasing zone of pore pressure gradually increases. (3) As the water-driven-methane process continues, the pore pressure along the driving direction gradually decreases. This is because the water pressure at the inlet is 0.7 MPa and the atmospheric pressure at the outlet is 0.1 MPa. The pore pressure in the coal is continuous from 0.7 MPa to 0.1 MPa, as shown in the cloud image of the pore pressure in Figure 11. (4) For the same point in space, the methane pressure in the coal sample gradually decreases over time. This is because the free methane in the coal sample is driven by water, resulting in a decrease in the free methane content and the methane pressure in the coal sample.

By combining the space-time distribution regularities of the pore pressure with the space-time distribution regularities of the water-methane two-phase saturation, it is concluded that the methane saturation in the decreasing zone of pore pressure is greater than that in the increasing zone of pore pressure. That is, the free methane content in the decreasing zone of pore pressure is greater than that in the increasing zone of pore pressure. This is because, in the increasing zone of pore pressure, some free methane is driven to the decreasing zone of pore pressure and some free methane is converted into adsorption methane. The free methane in the decreasing zone of pore pressure includes the free methane driven by water from the increasing zone of pore pressure, the original free methane in the region, and the free methane desorbed from the adsorbed methane.

5.2.2. Space-Time Distribution of the Pore Pressure on the Axial Line along the Driving Direction. The following can be seen from Figure 12 and Table 3. (1) The initial pore pressure in the coal sample is 0.5 MPa, and thus the initial pore pressure at each space point in the coal sample is 0.5 MPa. When the pressure water enters the coal sample, the free methane in the pores is driven forward and the pore pressure along the driving direction is redistributed. Therefore, the pore pressures at 10 mm, 20 mm, 30 mm, 40 mm, and 50 mm are all greater than the initial pore pressure, indicating that these points in space are located in the increasing zone of pore pressure. However, the pore pressures at 60 mm, 70 mm, 80 mm, and 90 mm are less than the initial pore pressure, indicating that these points in space are located in the decreasing zone of pore pressure. That is, the increasing zone of pore pressure is distributed closer to the water inlet end, and the decreasing zone of pore pressure is distributed closer to the methane outlet end. This is because the water inlet end is closer to

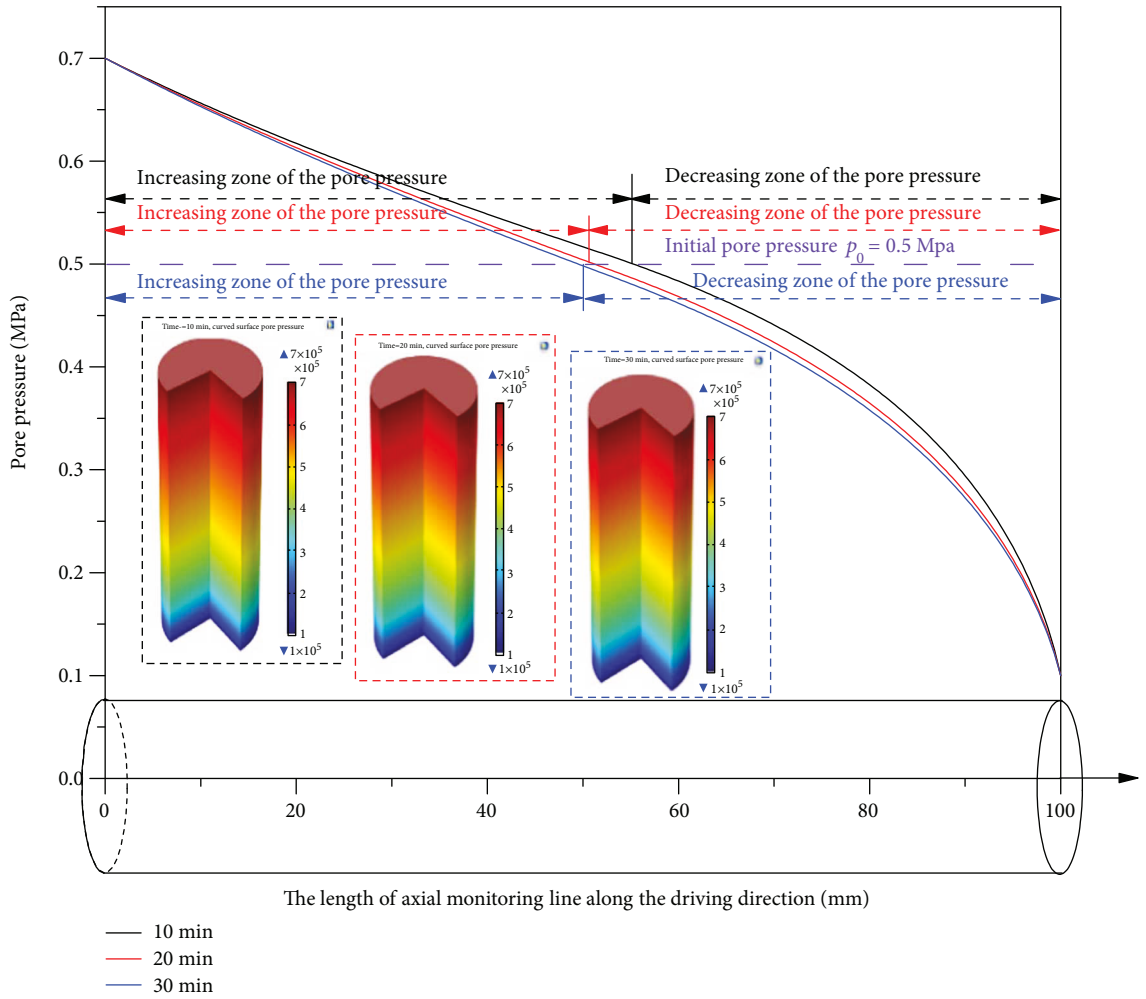

Figure 11: Space-time curve and cloud image of the pore pressure on the axial monitoring line along the driving direction.

a high-pressure source of 0.7 MPa, and the methane outlet end is closer to a low-pressure source of 0.1 MPa. (2) Over time, the pore pressure in the increasing zone first increases and then decreases, but the pore pressure in the decreasing zone decreases continuously. (3) At the beginning of the water-driven-methane process, the change (increase or decrease) rate of the pore pressure decreases from both ends to the middle of the coal sample. This is because the two ends of the coal sample are close to a high- or low-pressure source, which creates a pressure difference from the initial pore pressure. At the beginning of the water-driven-methane process, to realize the continuous distribution of the pore pressure in the coal sample, it is necessary to overcome this pressure difference in order to realize the connection and transition of the pore pressure in the coal sample.

5.3. Space-Time Distribution of the Pore Pressure Gradient along the Driving Direction. The following can be seen from Figure 13 and Table 4. (1) When time is constant, the pore pressure gradient on the monitoring line first decreases and then increases. The decreasing zone of the pore pressure gradient is located in the increasing zone of pore pressure, and the increasing zone of the pore pressure gradient is located in the decreasing zone of pore pressure. (2) At the time of 30 minutes, the pore pressure gradient at the methane outlet end is 7~9 times greater than that at the water inlet end. This indicates that the pore pressure gradient at the side of the methane outlet is greater than that at the side of the water inlet. This is because the pressure difference of 0.4 MPa between the initial pore pressure and the atmospheric pressure is greater than the difference of 0.1 MPa between the water pressure and the initial pore pressure. (3) Over time, the pore pressure gradient at the side of the water inlet increases, but the rate of increase decreases. For example, the rate of increase of 0.183 MPa/m in the pore pressure gradient at 10~20 min is greater than the rate of increase of 0.141 MPa/m in the pressure gradient at 20~30 min. (4) Over time, the pore pressure gradient at the side of the methane outlet decreases, and the rate of decrease decreases as well. For example, the rate of increase of 5.515 MPa/m in the pore pressure gradient at 10~20 min is greater than the rate of increase of 1.76 MPa/m in the pressure gradient at 20~30 min. (5) The rate of increase in the pore pressure gradient at the water inlet is less than the rate of decrease in the pore pressure gradient at the methane outlet.

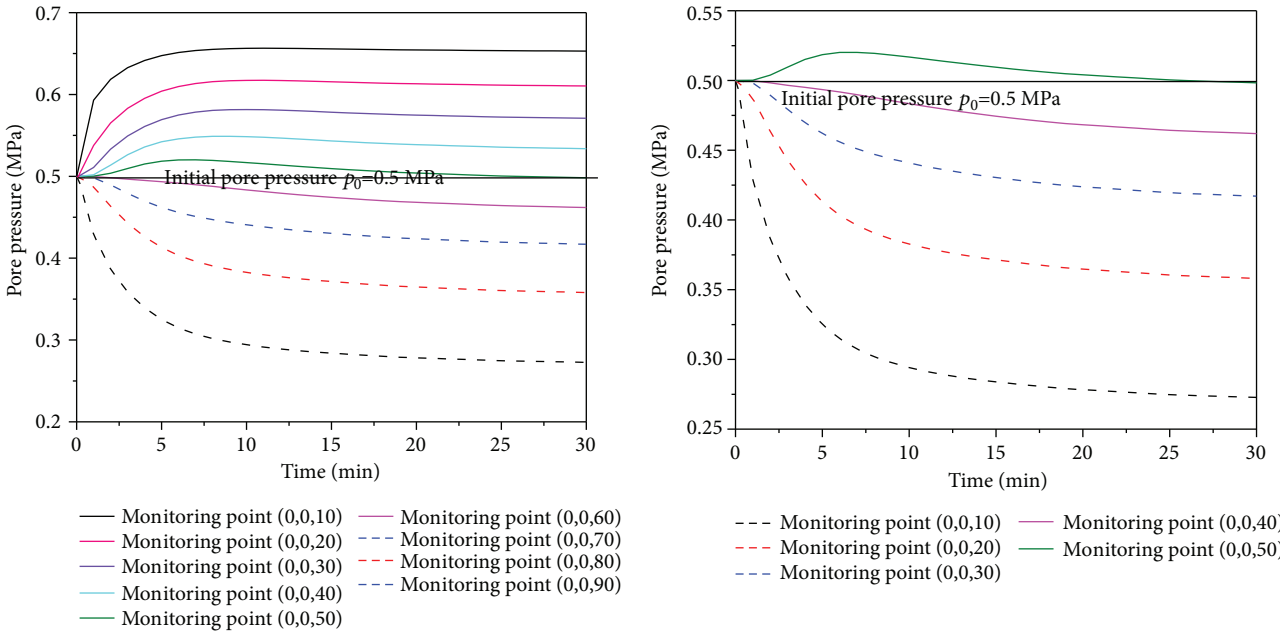

(a) Axial monitoring points at the positions of 10 mm, 20 mm, 30 mm, 40 mm, 50 mm, 60 mm, 70 mm, 80 mm, and 90 mm

(b) Axial monitoring points at the positions of 10 mm, 20 mm, 30 mm, 40 mm, and 50 mm

Figure 12: Space-time distribution curves of the pore pressure at the axial monitoring points along the driving direction.

Table 3: Space-time distribution of the pore pressure at the axial monitoring points.

Time (min)	Monitoring point (mm)								
	10 Pore pressure (MPa)	20 Pore pressure (MPa)	30 Pore pressure (MPa)	40 Pore pressure (MPa)	50 Pore pressure (MPa)	60 Pore pressure (MPa)	70 Pore pressure (MPa)	80 Pore pressure (MPa)	90 Pore pressure (MPa)
0	0.500	0.500	0.500	0.500	0.500	0.500	0.500	0.500	0.500
5	0.648	0.604	0.569	0.542	0.519	0.493	0.462	0.413	0.325
10	0.656	0.617	0.582	0.548	0.517	0.483	0.441	0.383	0.294
15	0.656	0.616	0.578	0.543	0.509	0.474	0.430	0.371	0.284
20	0.654	0.613	0.575	0.539	0.504	0.468	0.424	0.365	0.278

6. Conclusions

(1) Based on the conceptual model of methane driven by water in porous coal rock, with the effect of methane adsorption and desorption considered, a fluid-solid coupling mathematical model of methane driven by water is established in this paper. The accuracy and reliability of the mathematical model have been verified by the results of the water-driven-methane experiment in a briquette coal sample.

(2) With the help of the COMSOL Multiphysics software, visualization of the space-time distribution of water-methane two-phase saturation can be realized. The curve of the water saturation over time changes from a lower concave curve to a straight line, while the curve of the methane saturation with time changes from an upper convex curve to a straight line. Meanwhile, both of the increase rate of the water saturation and the decrease rate of the methane saturation gradually reduce over time.

(3) In the water-driven-methane process, the pore pressure of the coal sample is redistributed. The maximum pore pressure is the water pressure at the side of the water inlet, and the minimum pore pressure is the atmospheric pressure at the side of the methane outlet. The pore pressure decreases along the driving direction. Using the initial pore pressure as the dividing line, the coal sample can be divided into an increasing zone and a decreasing zone of pore pressure. The increasing zone of pore pressure is close to the side of the water inlet, and the decreasing zone of pore pressure is close to the methane outlet. The increasing zone of pore pressure gradually decreases, and the decreasing zone of pore pressure gradually

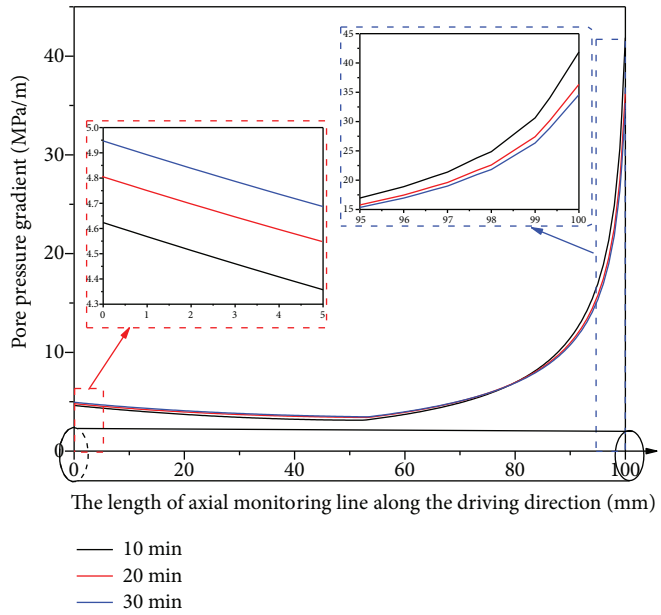

Figure 13: Space-time distribution of the pore pressure gradient along the driving direction.

Table 4: Space-time distribution of the pore pressure gradient at the axial monitoring points.

Time (min)	Monitoring point (mm)										
	0 Pore pressure (MPa/m)	10 Pore pressure (MPa/m)	20 Pore pressure (MPa/m)	30 Pore pressure (MPa/m)	40 Pore pressure (MPa/m)	50 Pore pressure (MPa/m)	60 Pore pressure (MPa/m)	70 Pore pressure (MPa/m)	80 Pore pressure (MPa/m)	90 Pore pressure (MPa/m)	100 Pore pressure (MPa/m)
10	4.623	4.119	3.720	3.422	3.225	3.135	3.719	4.893	6.946	11.455	41.869
20	4.806	4.325	3.966	3.704	3.526	3.423	3.930	5.049	6.944	10.963	36.354
30	4.947	4.460	4.091	3.817	3.622	3.497	3.981	5.071	6.899	10.751	34.594

increases. Over time, the pore pressure in the increasing zone of pore pressure first increases and then decreases, and the pore pressure in the decreasing zone of pore pressure continuously decreases. The change (increase or decrease) rate of the pore pressure in the coal sample gradually decreases from both ends towards the middle of the coal sample.

(4) The pore pressure gradient decreases first and then increases along the driving direction. The decreasing zone of the pore pressure gradient is located in the increasing zone of pore pressure, and the increasing zone of the pore pressure gradient is located in the decreasing zone of pore pressure. In the water-driven-methane process, the distribution of the pore pressure gradient is influenced by the difference between the initial pore pressure and the atmospheric pressure at the side of the methane outlet and the difference between the water pressure at the side of the water inlet and the initial pore pressure. When the pressure difference between the first two is greater than that between the latter two, the pore pressure gradient at the side of the methane outlet is greater than that at the side of the water inlet. Over time, the pore pressure gradient at the side of the water inlet increases, and its rate of increase decreases. The pore pressure gradient at the side of the methane outlet decreases, and its rate of decrease also decreases. The rate of increase in the pore pressure gradient at the side of the water inlet is greater than the rate of decrease in the pore pressure gradient at the side of the methane outlet.

Data Availability

The data used to support the findings of this study are available from the corresponding author upon request.

Conflicts of Interest

The authors declare that they have no conflicts of interest.

Acknowledgments

The financial support for this work, provided by the National Key Research and Development Program of China (no. 2017YFC0603001), the National Science Fund for Excellent Young Scholars (no. 51522406), and the Fundamental

Research Funds for the Central Universities (China University of Mining and Technology) (no. 2015XKZD04), is gratefully acknowledged.

References

[1] B. Huang, Q. Cheng, and S. Chen, "Phenomenon of methane driven caused by hydraulic fracturing in methane-bearing coal seams," *International Journal of Mining Science and Technology*, vol. 26, no. 5, pp. 919–927, 2016.

[2] Y. Ma, Y. Cheng, Z. Liu, and F. Cai, "Improvement of drainage gas of steep gassy coal seam with underground hydraulic fracture stimulation: a case in Huainan, China," *International Journal of Oil, Gas and Coal Technology*, vol. 13, no. 4, pp. 391–406, 2016.

[3] X. Xia, K. Lin, X. Lu et al., "Study of the effects of hydraulic fracturing at different dip angles for the development of coalbed methane: a case study in the southeast part of Qinshui Basin, China," *International Journal of Oil, Gas and Coal Technology*, vol. 14, no. 1/2, pp. 186–200, 2017.

[4] Y. Lu, Z. Yang, X. Li, J. Han, and G. Ji, "Problems and methods for optimization of hydraulic fracturing of deep coal beds in China," *Chemistry and Technology of Fuels and Oils*, vol. 51, no. 1, pp. 41–48, 2015.

[5] J. Xu, C. Zhai, and L. Qin, "Mechanism and application of pulse hydraulic fracturing in improving drainage of coalbed methane," *Journal of Natural Gas Science and Engineering*, vol. 40, no. 4, pp. 79–90, 2017.

[6] H. Zhang, Y. Cheng, Q. Liu et al., "A novel in-seam borehole hydraulic flushing gas extraction technology in the heading face: enhanced permeability mechanism, gas flow characteristics, and application," *Journal of Natural Gas Science and Engineering*, vol. 46, no. 10, pp. 498–514, 2017.

[7] L. Yanwei, W. Qian, C. Wenxue, L. Mingju, and H. Mitri, "Enhanced coalbed gas drainage based on hydraulic flush from floor tunnels in coal mines," *International Journal of Mining, Reclamation and Environment*, vol. 30, no. 1, pp. 37–47, 2016.

[8] F. Yan, B. Lin, C. Zhu et al., "A novel ECBM extraction technology based on the integration of hydraulic slotting and hydraulic fracturing," *Journal of Natural Gas Science and Engineering*, vol. 22, no. 1, pp. 571–579, 2015.

[9] X. G. Zhang, P. G. Ranjith, M. S. A. Perera, A. S. Ranathunga, and A. Haque, "Gas transportation and enhanced coalbed methane recovery processes in deep coal seams: a review," *Fuel*, vol. 30, no. 11, pp. 8832–8849, 2016.

[10] Z. Liu and H. Wu, "Pore-scale modeling of immiscible two-phase flow in complex porous media," *Applied Thermal Engineering*, vol. 93, no. 1, pp. 1394–1402, 2016.

[11] J. Liu, J. G. Wang, F. Gao, Y. Ju, X. Zhang, and L. C. Zhang, "Flow consistency between non-Darcy flow in fracture network and nonlinear diffusion in matrix to gas production rate in fractured shale gas reservoirs," *Transport in Porous Media*, vol. 111, no. 1, pp. 97–121, 2016.

[12] A. Basu, M. J. Boyd, and P. McConchie, "Numerical modelling of two phase flow of gas and water during drainage of a coal seam," *International Journal of Mine Water*, vol. 7, no. 4, pp. 27–42, 1988.

[13] J. Liu, "Simulation of coal-bed methane and water two-phase fluid-solid coupling flow," in *ISRM International Symposium/2nd Asian Rock Mechanics Symposium (ISRM 2001-2nd ARMS)*, Beijing, China, 2001http://xueshu.baidu.com/s?wd=paperuri%3A%282e06c1c106802a97301dbebc58415eea%29&filter=sc_long_sign&tn=SE_xueshusource_2kduw22v&sc_vurl=http%3A%2F%2Fwww.onepetro.org%2Fconference-paper%2FISRM-ARMS2-2001-077&ie=utf-8&sc_us=2708211531915967481.

[14] S. Li, C. Fan, J. Han, M. Luo, Z. Yang, and H. Bi, "A fully coupled thermal-hydraulic-mechanical model with two-phase flow for coalbed methane extraction," *Journal of Natural Gas Science and Engineering*, vol. 33, no. 7, pp. 324–336, 2016.

[15] S. K. Chen, T. H. Yang, and C. H. Wei, "Displacement mechanism of the two-phase flow model for water and gas based on adsorption and desorption in coal seams," in *International Symposium on Multi-field Coupling Theory of Rock and Soil Media and Its Applications*, Chengdu, China, 2010http://www.wanfangdata.com.cn/details/detail.do?_type=conference&id=WFHYXW399133.

[16] H. Liu, J. Mou, and Y. Cheng, "Impact of pore structure on gas adsorption and diffusion dynamics for long-flame coal," *Journal of Natural Gas Science and Engineering*, vol. 22, no. 1, pp. 203–213, 2015.

[17] L. Si, Z. Li, Y. Yang et al., "Experimental investigation for pore structure and CH_4 release characteristics of coal during pulverization process," *Energy & Fuels*, vol. 31, no. 12, pp. 14357–14366, 2017.

[18] S. Hou, X. Wang, X. Wang, Y. Yuan, S. Pan, and X. Wang, "Pore structure characterization of low volatile bituminous coals with different particle size and tectonic deformation using low pressure gas adsorption," *International Journal of Coal Geology*, vol. 183, no. 1, pp. 1–13, 2017.

[19] H. Guo, Y. Cheng, T. Ren et al., "Pulverization characteristics of coal from a strong outburst-prone coal seam and their impact on gas desorption and diffusion properties," *Journal of Natural Gas Science and Engineering*, vol. 33, no. 7, pp. 867–878, 2016.

[20] H. Guo, Y. Cheng, L. Yuan, L. Wang, and H. Zhou, "Unsteady-state diffusion of gas in coals and its relationship with coal pore structure," *Energy & Fuels*, vol. 30, no. 9, pp. 7014–7024, 2016.

[21] J. Wu, J. Wang, J. Liu et al., "Moisture removal mechanism of low-rank coal by hydrothermal dewatering: physicochemical property analysis and DFT calculation," *Fuel*, vol. 187, no. 1, pp. 242–249, 2017.

[22] L. Wang, E. T. Chen, S. Liu et al., "Experimental study on the effect of inherent moisture on hard coal adsorption–desorption characteristics," *Adsorption*, vol. 23, no. 5, pp. 723–742, 2017.

[23] Y. Wen, J. Liao, X. Liu, F. Wei, and L. Chang, "Removal behaviors of moisture in raw lignite and moisturized coal and their dewatering kinetics analysis," *Drying Technology*, vol. 35, no. 1, pp. 88–96, 2017.

[24] Z. Zhang, "Structure and dynamics in brown coal matrix during moisture removal process by molecular dynamics simulation," *Molecular Physics*, vol. 109, no. 3, pp. 447–455, 2011.

[25] J. Shaikh, A. Sharma, and R. Bhardwaj, "On comparison of the sharp-interface and diffuse-interface level set methods for 2D capillary or/and gravity induced flows," *Chemical Engineering Science*, vol. 176, no. 2, pp. 77–95, 2018.

[26] Q. Q. Liu, Y. P. Cheng, W. Li, and W. Zhao, "Mathematical model of coupled gas flow and coal deformation process in low-permeability and first mined coal seam," *Chinese Journal of Rock Mechanics and Engineering*, vol. 34, no. 1, pp. 2749–2758, 2015.

[27] C. J. Fan, S. Li, M. K. Luo, Z. Yang, H. Zhang, and S. Wang, "Deep CBM extraction numerical simulation based on hydraulic-mechanical-thermal coupled model," *Journal of China Coal Society*, vol. 41, no. 12, pp. 3076–3085, 2016.

[28] L. D. Connell, M. Lu, and Z. Pan, "An analytical coal permeability model for tri-axial strain and stress conditions," *International Journal of Coal Geology*, vol. 84, no. 2, pp. 103–114, 2010.

[29] L. D. Connell, "A new interpretation of the response of coal permeability to changes in pore pressure, stress and matrix shrinkage," *International Journal of Coal Geology*, vol. 162, no. 5, pp. 169–182, 2016.

[30] J. Chen, J. W. Hopmans, and M. E. Grismer, "Parameter estimation of two-fluid capillary pressure–saturation and permeability functions," *Advances in Water Resources*, vol. 22, no. 5, pp. 479–493, 1999.

[31] M. Yi, P. Guo, and L. Sun, "An experimental study on relative permeability curve for unsteady-state gas displacement by water," *Natural Gas Industry*, vol. 27, no. 10, pp. 92–94, 2007, http://xueshu.baidu.com/s?wd=paperuri%3A%281d1009acc62bded12bd3d6d1f6ed0ed4%29&filter=sc_long_sign&tn=SE_xueshusource_2kduw22v&sc_vurl=http%3A%2F%2Fkns.cnki.net%2FKCMS%2Fdetail%2Fdetail.aspx%3Ffilename%3Dtrqg200710031%26dbname%3DCJFD%26dbcode%3DCJFQ&ie=utf-8&sc_us=12331676811207054247.

[32] Y. Gensterblum, A. Busch, and B. M. Krooss, "Molecular concept and experimental evidence of competitive adsorption of H_2O, CO_2 and CH_4 on organic material," *Fuel*, vol. 115, no. 4, pp. 581–588, 2014.

[33] X.-Q. Liu, X. He, N. X. Qiu et al., "Molecular simulation of CH_4, CO_2, H_2O and N_2 molecules adsorption on heterogeneous surface models of coal," *Applied Surface Science*, vol. 389, no. 12, pp. 894–905, 2016.

[34] J. Xiang, F. G. Zeng, H. Z. Liang, B. Li, and X. X. Song, "Molecular simulation of the $CH_4/CO_2/H_2O$ adsorption onto the molecular structure of coal," *Science China Earth Sciences*, vol. 57, no. 8, pp. 1749–1759, 2014.

[35] S. Yu, J. Bo, and L. Wu, "Molecular simulation of $CH_4/CO_2/H_2O$ competitive adsorption on low rank coal vitrinite," *Physical Chemistry Chemical Physics*, vol. 19, no. 27, pp. 17773–17788, 2017.